Direct atomic imaging of Ag(100) and Ag(111) by inverting quasielastically scattered electron-diffraction patterns

P. R. Jeng, I. H. Hong, and Y. C. Chou
Department of Physics and Material Science Center, National Tsing-Hua University, Hsinchu, Taiwan 30043, Republic of China

C. M. Wei
Institute of Physics, Academia Sinica, Nankang, Taipei, Taiwan 11529, Republic of China
(Received 8 September 1994; revised manuscript received 30 November 1994)

Direct imaging of three-dimensional atomic structure of Ag(100) and Ag(111) surfaces by Fourier-transforming the multiple-energy diffraction patterns of quasielastically scattered electrons is demonstrated experimentally. The holographic images obtained with an integral-energy phase-summing method are of high fidelity and free from artifacts. The resolution of the atomic images is ~ 1 Å in all spatial directions. The atoms down to three layers below the emitters are three dimensionally imaged. The contribution from backward-scattering and forward-scattering oscillations can be separately observed by varying the energy range used in Fourier transformation. The surface sensitivity can be enhanced by using an off-normal-incident geometry. With a limited energy range (~ 200 eV) used in Fourier transformation, the atoms behind the emitter in the backward direction are observed.

I. INTRODUCTION

Electron-emission holography (EEH),[1-9] which refers to direct reconstruction of electron-diffraction patterns to produce three-dimensional atomic images around a local electron source in a solid surface, has attracted much attention of many research groups. The angular distribution of emitted electrons, resulting from the interference between a direct wave (reference wave) from the emitter and a scattered wave (object wave) off the neighboring atoms, can be considered as a hologram. There are many kinds of emitted electrons, such as photoelectrons,[1-3] Auger electrons,[4,5] DLEED (diffuse low-energy electron-diffraction) electrons,[6,7] and quasielastically scattered (Kikuchi) electrons,[8,9] which can be used in the holographic studies.

The aim of electron-emission holography is to develop a direct method for surface structural determination[10,11] which should have the following three characteristics. First, only a simple Fourier transform is needed to reconstruct the surface structure. Second, neither trial-and-error processes of structural modeling nor knowledge of scattering factors of constituent atoms are needed. Third, reconstructed images are free from artifacts. However, most previous experimental results in this research area failed to met the third characteristic.

In an original paper, Barton[1] performed a two-dimensional Fourier transformation on a simulated single-energy photoelectron-diffraction pattern from a S(1*s*) core level and obtained reconstructed images closely related to the surface structure of a $c(2\times 2)$ S/Ni(001) system. Since then, many experimental works were performed on the reconstruction of photoelectrons,[2,3] Auger electrons,[4,5] diffuse LEED,[7] and Kikuchi electron-diffraction patterns.[8] In these early studies, a two-dimensional Fourier transform was performed on the diffraction pattern of electrons at single energy. All these single-energy experiments[2-5,7,8] and simulations[1,6] suffered disadvantages such as artifacts, twin images, and shifts from correct positions, and had very poor resolution in the bond direction. As a result, a correction due to a strong atomic scattering phase shift has to be done on a single-energy diffraction pattern to obtain the image at the correct atomic position.[12-14] It was then realized[9-11,15-19] that multiple-energy diffraction patterns are needed to eliminate artifacts due to multiple-scattering effects and twins. Two different methods were developed to correct the multiple-scattering effects proposed by Tong and co-workers[10,11,15] and Barton.[16] Here we shall adapt the method developed by Tong and co-workers;[10,11] a comparison between the two methods is published elsewhere.[20]

In this paper, by using integral-energy phase summing, we demonstrate that direct Fourier inversion of measured quasielastically scattered electron (Kikuchi electron)-diffraction patterns of the Ag(100) and Ag(111) surfaces shows clear three-dimensional (3D) atomic images of nearby atoms viewed from the emitters. The atoms down to three layers below the emitters can be three dimensionally imaged. No further treatment of the phase factor in the diffraction patterns or *a priori* knowledge of the surface structure is needed. The images of the atoms in both forward and backward directions can be obtained by varying the energy range and energy grid used in Fourier inversion.[9] Using off-normal-incident geometry, one is able to enhance the surface sensitivity. With a limited energy range used in the Fourier transformation, the atoms behind the emitter in the backward direction are observed.[21] Only laboratory LEED optics is used in our experiment, and the time span of data acquisition and data processing is short compared with other types of experiments, such as angular-resolved x-ray photoelectron spectroscopy (ARXPS),[2,3,18,19] angular-resolved Auger electron spectroscopy (ARAES),[4,5] and diffuse LEED,[7]

in the electron-emission holography.

Section II describes experimental details. In Sec. III, the integral-energy phase-summing method used to invert multiple-energy Kikuchi patterns is summarized. The results of Ag(100) and Ag(111) are presented in Sec. IV. The contribution to the reconstructed images from forward and backward scattering is discussed in Sec. V. Special characteristics of an off-normal-incident experiment are presented. The prospect of EEH using an electron beam as an excitation source is summarized in Sec. VI.

II. EXPERIMENT

A. Sample preparation

The single-crystal Ag(100) and Ag(111) surfaces of high purity (99.999%) were mechanically polished and chemically etched before being inserted into the load-locking chamber (with a pressure of $<2\times10^{-8}$ torr), attached to a sample preparation chamber. In this sample preparation chamber (with a base pressure of $<2\times10^{-10}$ torr), there are an ion-sputtering gun, a four-grid LEED/Auger optics, and a glancing incidence electron gun for AES studies.

The single-crystal surfaces were cleaned by repeated cycles of Ar^+ sputtering (500-V, 5×10^{-5}-torr Ar) and annealing to 500 °C with resistive heating. The surfaces were considered clean when sharp 1×1 LEED spots with a low background were observed, and AES showed no carbon, sulfur, or oxygen contamination. A single crystal with a clean and well-ordered surface was then transferred into a μ-metal analyzing chamber under the pressure $<4\times10^{-10}$ torr.

B. Data acquisition

The measurements of Kikuchi patterns (Kikuchi electron holograms) were performed in this μ-metal UHV analyzing chamber with a base pressure less than 1×10^{-10} torr, equipped with a three-grid rear-view LEED optics, a two-axis ratable hemispherical analyzer, a twin anode x-ray tube, and an UV lamp.

Kikuchi patterns with normally (the polar angle is 0°, i.e., along the surface normal [100]) and off-normally (the polar angle is 26°, from the surface normal toward [011] along the surface mirror plane) incident electron beams were collected at a display-type LEED screen (the angle of acceptance from the sample is 104°) and recorded with a charge-coupled device (CCD) camera (8-bit gray level, 512×480 pixels). The recorded diffraction pattern was then binned to result in a format of 108×108 pixels per image. The angular resolution of this detector is less than ±0.5°/pixel. Each pattern for every beam energy was repeatedly measured ten times. These data were then added together and averaged with a symmetry-equivalence operation to improve the signal-to-noise ratio.

The data-acquisition processes were controlled by a personal computer and the results were digitally stored for further analysis. The electron-emission angles are carefully calibrated with the positions of the LEED spots. A series of 47 Kikuchi patterns was taken for an Ag(100) surface with an incident electron beam energy range from 229 to 557 eV, and a set of more than 160 patterns was recorded for an Ag(111) surface with an incident electron beam energy ranging from 218 to 1942 eV. Both data sets were taken in an equal electron wave-number increment of $\Delta k=0.05$ a.u.$^{-1}$ A total acquisition time of 47 Kikuchi patterns needs 1 h. We also measured the Kikuchi patterns of an Ag(100) surface with different suppressor energy filters at 12, 20, 35, and 70 eV for comparison. The probing depth of the 12-eV experiment seems to be longer than that of the high suppressor energy experiments. Otherwise the images are independent of the suppressor energy. The data obtained are highly reproducible in different runs of experiments.

III. INTEGRAL-ENERGY PHASE-SUMMING METHOD (IEPSM)

Tong and co-workers[10,17] and Wei and co-workers[9,11] extended the idea of energy-dependent photoelectron diffraction (EDPD),[22] and used the integral-energy phase-summing method (IEPSM) to eliminate artifacts and suppress twins to obtain a high-fidelity 3D atomic image.

In IEPSM, the normalized scan-energy modulation $\chi(\mathbf{k}_f)$ of the electron intensity is Fourier transformed with respect to the vector position $\mathbf{R}$:

$$\phi_{\mathbf{k}_f}(\mathbf{R})=\int_{k_{\min}}^{k_{\max}}\chi(\mathbf{k}_f)e^{-ik_fR}e^{i\mathbf{k}_f\cdot\mathbf{R}}k_f^2dk_f\ , \tag{1}$$

where $\mathbf{R}$ is the 3D position vector of a nearby atom with its origin at the emitter, and the normalized modulation $\chi(\mathbf{k}_f)$ for each direction $\hat{k}_f$ is normalized as $\chi(\mathbf{k}_f)=I(\mathbf{k}_f)/I_a(\mathbf{k}_f)-1$. The procedure[9,23] to obtain $\chi(\mathbf{k}_f)$ is the following: (i) Obtain the intensity spectrum $I(\mathbf{k}_f)$ as a function of energy for each emission direction $\hat{k}_f$ in the selected energy range, (ii) $I(\mathbf{k}_f)$ is least square fitted by a low-order (first or second order) polynomial $I_a(\mathbf{k}_f)$ in the range $k_{\min}<k_f<k_{\max}$, and $\mathbf{k}_f$ is the wave vector of outgoing electrons; thus $\chi(\mathbf{k}_f)$ is obtained for the $\hat{k}_f$ direction.

The complex Fourier amplitudes of Eq. (1) are then summed over a span of emission direction $\hat{k}_f$:

$$\Phi(\mathbf{R})=\sum_{\hat{k}_f}\phi_{\hat{k}_f}(\mathbf{R})\ . \tag{2}$$

The real-space image is obtained by evaluating the absolute quantities $|\Phi(\mathbf{R})|^2$ or $|R\Phi(\mathbf{R})|^2$ in three-dimensional $\mathbf{R}$ space, where the local maximums indicate the atomic positions near the emitters.

IEPSM (Refs. 9–11) is similar to EDPD.[22] The main difference is that the single-scattering pattern difference ξ used in EDPD is replaced by $(R-\hat{k}\cdot\mathbf{R})$ in IEPSM. It is this key difference which give us the bond-angle as well as the bond-length information. Thus, the complete 3D atomic structure can be determined directly.

IV. RESULTS OF Ag(100) AND Ag(111) SURFACES

Figure 1(a) shows six Kikuchi patterns of an Ag(100) surface at different incident electron beam energies. The

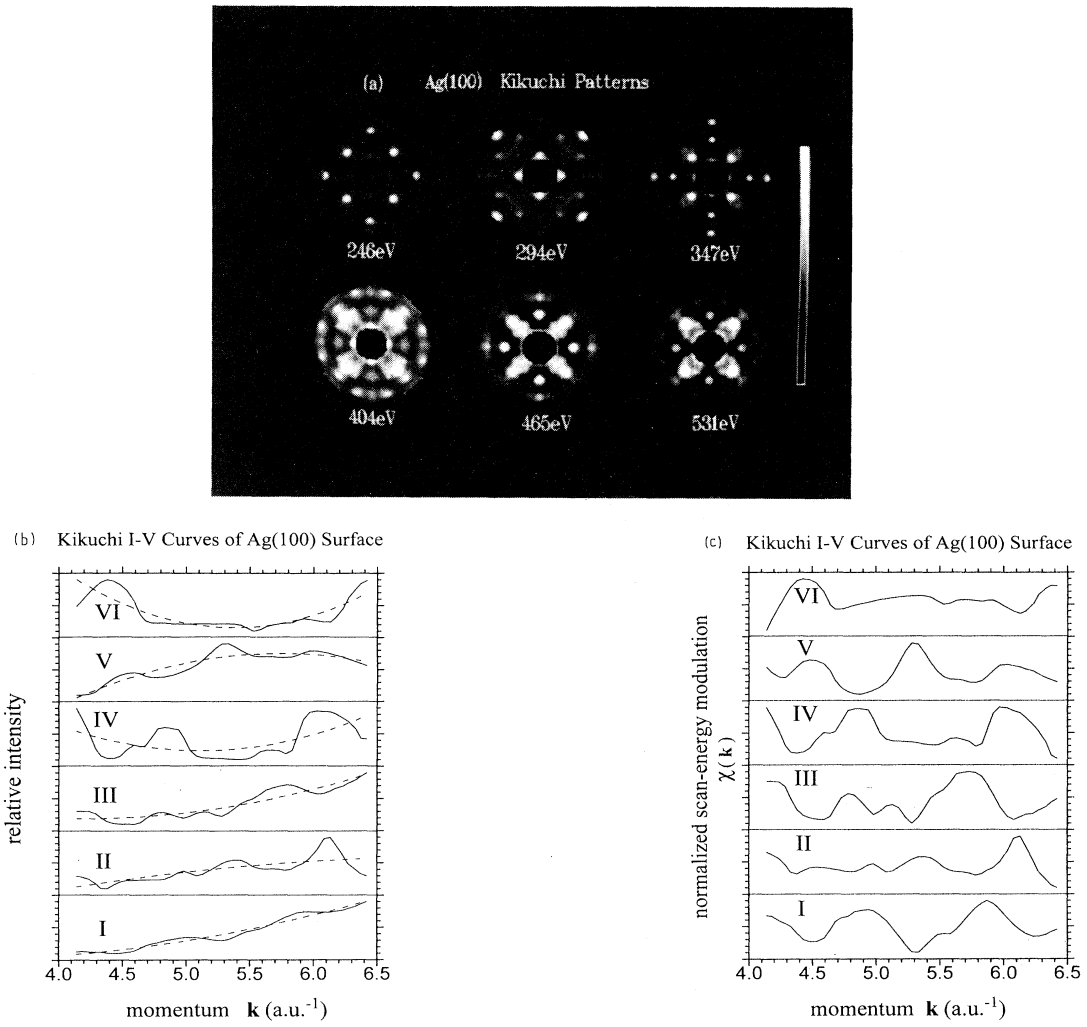

FIG. 1. (a) Six Kikuchi patterns of the Ag(100) surface at different incident energies. These patterns are displayed in an orthographic projection, with the polar angles ranging from 10° to 52°. Each pattern is fourfold symmetry averaged. The big black dot at the center of each pattern is the shadow of the electron gun. (b) The measured Kikuchi intensity spectra $I(\mathbf{k}_f)$ (solid lines) for the Ag(100) surface at six different emission directions, i.e., (I) $\varphi=0°$, $\vartheta=12.5°$; (II) $\varphi=0°$, $\vartheta=32.5°$; (III), $\varphi=15°$, $\nu=17.5°$; (IV) $\varphi=15°$, $\vartheta=37.5°$; (V) $\varphi=30°$, $\vartheta=12.5°$; and (VI) $\varphi=35°$, $\vartheta=32.5°$. The backgrounds $I_a(\mathbf{k}_f)$ (dashed lines) fitted with the second-order polynomial. (c) The normalized intensity modulations $\chi(\mathbf{k}_f)$ of Kikuchi electrons for the Ag(100) surface at the same six emission directions reported in (b).

suppressor voltage used is 12 eV. The patterns shown in Fig. 1(a) are the angular anisotropy of the Kikuchi patterns. It is clear that the angular anisotropy is strongly dependent on the incident electron beam energy. Figure 1(b) shows the intensities of the Kikuchi electrons $I(\mathbf{k}_f)$ as functions of the momentum of the electrons at six different directions (solid lines). The dashed lines in Fig. 1(b) are the second-order polynomial backgrounds $I_a(\mathbf{k}_f)$ obtained by using a least-squares-fit method to fit $I(\mathbf{k}_f)$. The normalized scan-energy modulation $\chi(\mathbf{k}_f)$ for individual directions is obtained according to the definition described in Sec. III. The normalized modulations $\chi(\mathbf{k}_f)$ at the same six emission directions described in Fig. 1(b) are shown in Fig. 1(c). We then use the integral-energy phase-summing method to direct Fourier transform these measured Kikuchi patterns. Zhao *et al.*[24] performed similar Kikuchi electron experiments. However, they only analyzed the data in the high-energy (> 500 eV) range where forward focusing effects dominated, and they did not perform Fourier transformation to obtain direct atomic image.

Figures 2(a)–2(c) show top views of the reconstructed images of the atoms at 1–3 layers below the emitter. The images are reconstructed from eight Kikuchi patterns with incident electron energies from 313 to 465 eV. The number of Kikuchi patterns used here is the minimum number of patterns that gives clear atomic images. Generally speaking, increasing the number of Kikuchi pat-

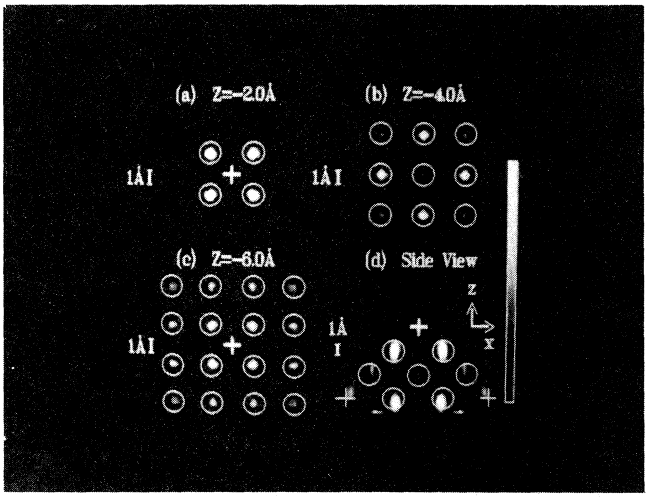

FIG. 2. The top-view atomic images of the Ag(100) surface below the emitter at (a) 2.0 Å, (b) 4.0 Å, and (c) 6.0 Å. (d) The side-view reconstructed image of the Ag(100) surface cut through the (001) plane of the images shown in (a)–(c). Complete 3D holographic images are shown in Fig. 4(a).

terns in the image reconstruction will increase the resolution of the image, as can be seen in Fig. 3. The reconstructed atomic layer spacing is 2.0 Å. Figure 2(d) shows the side-view image cut through the emitter and along the [010] direction. Centers of the circles and thin crosses mark the correct atomic positions. The thick cross marks the position of emitter, or marks the projection of the position of emitter if $z<0$. The images are free from artifacts and without twins. The resolution in the bond direction is ~ 1 Å, and thus provides the high resolution in any direction. The intensities of the atomic images in different layers are normalized so that the maximum intensity in 3D real space is 255. The shadow of the electron gun of the LEED apparatus blocks the electrons backscattered from the atom right below the emitter, so that the intensity of the image at the center of Fig. 2(b) is reduced. It is also observed that the number of atomic images is found to increase toward the bulk. The reason might be that, in the limited energy range, only atoms in the backscattering cone and within the mean free path of electrons can be imaged. The area covered by the backscattering cone increases toward the bulk, so the number of imaged atoms increases. The phase relation between the reference wave and the object wave will be scrambled if unwanted inelastic-scattering events occur in the paths along emitter to scatterer and scatterer to the surface. As a result, the maximum observable depth is limited by half of the mean free path of the electrons.

One of the merits of the holographic technique is that the three-dimensional (3D) atomic image can be directly inverted from the diffraction patterns of the emitted electrons. Also, good images in some cut planes do not guarantee that the same occurs in other cut planes. Hence it is worthwhile to present the whole 3D atomic image and to compare the image with the real-space atomic structure model. Figure 4(a) shows the 3D reconstruction of the atomic image of the Ag(100) surface. The 3D images are composed of the 40 top-view images

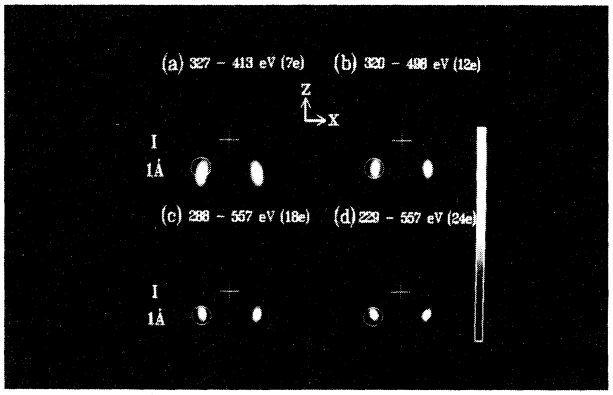

FIG. 3. Atomic images of the Ag(100) surface for various numbers of Kikuchi patterns in the image reconstruction.

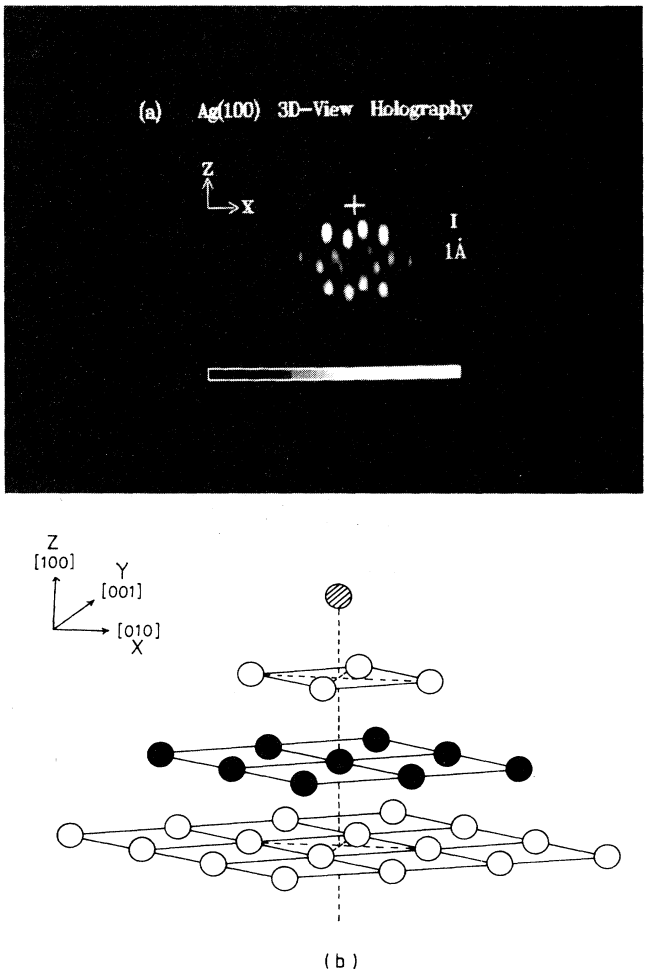

FIG. 4. (a) The 3D view of atomic images of the Ag(100) surface reconstructed from eight Kikuchi patterns (313–465 eV). Atoms down to three layers below the emitter (marked by thick cross) are observed. (b) The 3D view of the atomic structural diagram of the Ag(100) surface.

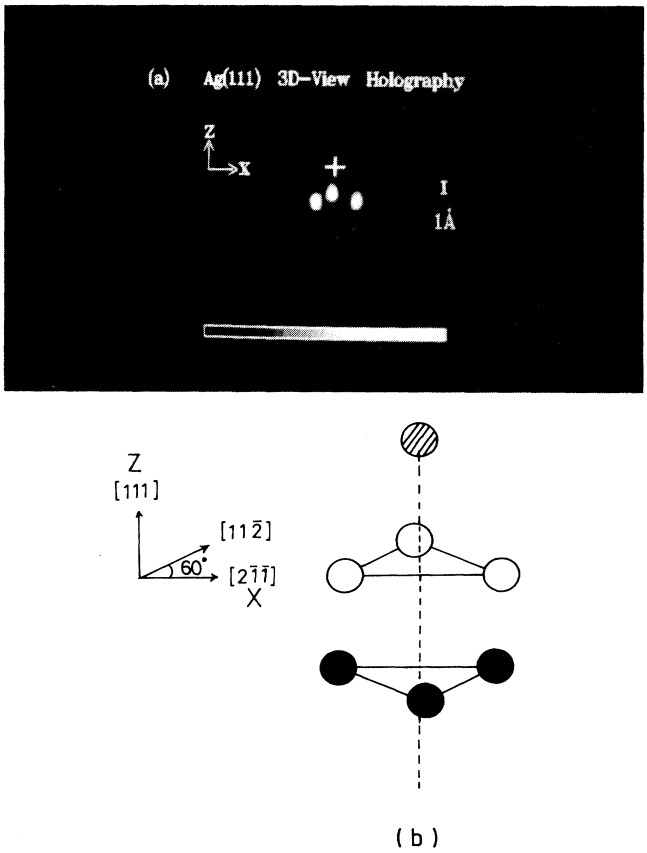

FIG. 5. (a) The 3D view of atomic images of the Ag(111) surface reconstructed from 11 Kikuchi patterns (300–548 eV). (b) The 3D view of the atomic structural diagram of the Ag(111) surface.

where the intensities of the constructed images are calculated for the planes from $z=+4.11$ to -6.85 Å, with a vertical spacing of 0.274 Å between each consecutive image plane. The plane including the emitter is at $z=0.0$ Å, and the backward direction is at $z<0$. Figure 4(b) shows the 3D atomic structure model, viewed from the same direction as that of Fig. 4(a), of the Ag(100) surface in the backward direction; the atoms are assumed to be at the bulk positions. It can be seen that the 3D reconstructed atomic image agrees very well with the 3D atomic structure model.

The same procedure is used to study the Ag(111) surface. Figure 5(a) shows the 3D atomic image of the local structure below the emitter. The 3D atomic images are reconstructed from 11 Kikuchi patterns with incident energies from 300 to 548 eV. Again, the 3D reconstructed atomic image corresponds very well to the atomic model shown in Fig. 5(b).

V. DISCUSSION

In the above, we have shown that 3D local atomic structures of Ag(100) and Ag(111) surfaces, by direct Fourier transformation of the multiple-energy Kikuchi

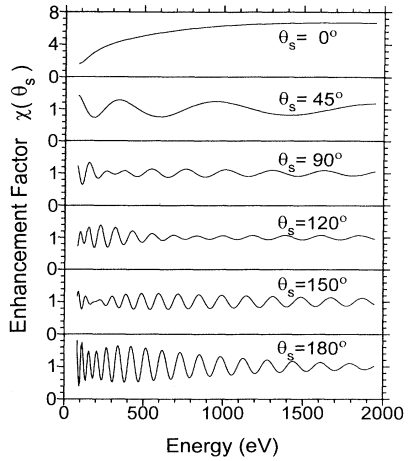

FIG. 6. Enhancement factors $\chi(\theta_s)$ at six different scattering angles θ_S calculated with the small-atom approximation for two Ag atoms 2.89 Å apart.

patterns, are of atomic resolution, free from artifacts and twins, and correct in the atomic position.

However, there are several points that need to be clarified. First, in all the atomic images reported above, only the images of atoms below the emitter, i.e., in the backward direction, are observed. This is due to the fact that only a limited energy range is used in reconstructing the atomic images. The atoms in the forward direction, i.e., the atoms above the emitter, can only be imaged if a wide energy range is used in the image reconstruction.[9] To illustrate this point, in Fig. 6 we show the calculated enhancement factor $\chi(\theta_s)$, where the scattering angle θ_s is defined as the polar angle between the bond direction and the direction of detection[25] of the forward ($\theta_s=0°$, 45°, and 90°) and backward ($\theta_s=120°$, 150°, and 180°) scattering as a function of electron energy in a two-Ag-atom system using small-atom approximation.[25] It is found that $\chi(\theta_s)$ in the forward-scattering cone is much less oscillatory than that in the backward-scattering cone. Thus, if the energy range used in the experiment is not wide enough to cover the slow intensity oscillation of the outgoing electrons in the forward direction, in our analysis scheme the contribution of the forward scattering is featureless and subtracted along with the background. This explains why we did not observe any image of atoms above the emitter in the forward direction, when the data for a limited energy range (313–465 eV) were used.

To further prove the correctness of this point and obtain a significant contribution from the forward scattering, we analyze the data in a wider energy range of 229 to 548 eV. Figure 7 shows a side-view image along the (001) plane of the Ag(100) surface. It is clear that both backward- and forward-scattering images are present at the same time. The resolution of the forward-scattering images is also less than those of the backward-scattering images, because the number of oscillations covered by the energy range of the experiment in the forward direction is less than the number of oscillations in the backward

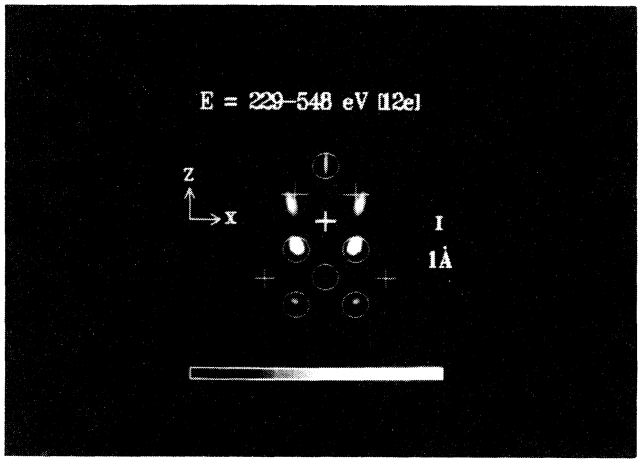

FIG. 7. Side-view atomic images along the (001) plane of the Ag(100) surface reconstructed with a wider energy range of 229–548 eV. Both the backward- and forward-scattering atomic images are observed.

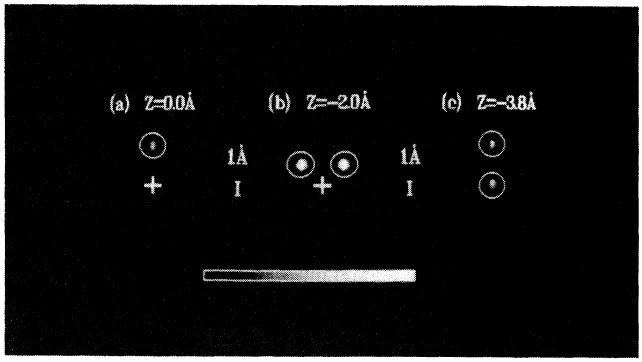

FIG. 8. The top-view atomic images of the Ag(100) surface below the emitter for an off-normal incident geometry (see the text). Panels (a)–(c) correspond to three different layers: (a) at 0.0 Å, (b) at 2.0 Å, and (c) at 3.8 Å. These images are reconstructed from 11 Kikuchi patterns (234–457 eV).

direction. The images in Figs. 2, 4, 5, and 7 confirm the idea that extracting the forward-scattering information requires performing the experiment over a wide energy range, while for the backward scattering a fine energy grid is needed. A detailed theoretical discussion has been presented in Ref. 23.

Second, to image the atoms in the topmost layer of surface with Kikuchi electron holography, the capability of imaging the atoms in the emitter plane[21,23,26] (or the same plane as the emitter, i.e., $z=0$) must be demonstrated. For the normal-incident geometry, electrons scattered from the atoms in the emitter plane and collected by LEED optics have scattering angles θ_s between 38° and 142°. Viewed from Fig. 6, for most of the above scattering angles, the intensity oscillation as a function of the energy is not fast enough. For the same reason presented above, the forward-scattering images cannot be revealed when a limited energy range (100–200 eV) is used in the holographic reconstruction. Thus electrons scattered from nearby atoms in the emitter plane do not contribute in the results of Fourier transformation with a finite energy range.

As we found in Sec. IV, one way to avoid such a difficulty is to collect the Kikuchi patterns for a large energy range of the incident electron. Another way is to increase the collection of the backward scattered electrons deliberately by rotating the sample to an off-normal incident geometry (with an incidence angle of 26° in the [011] direction). Figures 8(a), 8(b), and 8(c) show top-view images at $z=0.0$ Å (emitter plane), -2.0 Å (one layer below the emitter) and -3.8 Å (two layers below the emitter). These holographic images are reconstructed with the 11 incident energies from 234 to 457 eV. The bright spot in Fig. 8(a) corresponds to the atom at an ideal radial distance of 2.84 Å in the emitter plane and behind the emitter in the direction of incidence. In other words, one can increase the surface sensitivity in an off-normal configuration.[21,23,26] The bright spots in Fig. 8(b) correspond the two nearest-neighboring atoms in the layer just below the emitter, which are the same images of the atoms shown in Fig. 2(a). The bright spots in Fig. 8(c) correspond to the two second-neighboring atoms in the second layer below the emitter, which also are the same images of the atoms shown in Fig. 2(b), and behind the emitter in the direction of incidence. All the image spots appear at the correct atomic positions with an accuracy of ±0.4 Å. The fourfold symmetry in the normal-incidence geometry is now broken in an off-normal geometry, and some atoms in the emitter plane are imaged with our experimental setup. The other atoms in the forward-scattering direction cannot be imaged in our experiments for the reason given above. This is rather advantageous in that one can select to image the atoms behind the emitter in an experimentally specified measured direction. This directional selection rule has also been proved for the holographic studies of Si(001)-2×1 reconstructed surface.[21,23,26] There is also a different directional selection rule proposed by Hofmann *et al.*,[27] which requires aligning the angular-resolved detector exactly along the scatterer-emitter bond direction. However, the resolution in the direction perpendicular to the bond direction is very poor using their method.[27]

Third, the surface sensitivity is an inherent property of Kikuchi electron holography in the glancing incident detection configuration. It is not necessary to choose a particular energy range to minimize the mean free path so as to increase the surface sensitivity. We believe that the contribution to the image observed in the emitter plane [Fig. 8(a)] most likely comes from the scattering in the outermost few layers of the Ag(100) surface. The angle of the incident detection configuration is the key factor to determine the depth of probe. Such an argument is supported by the observation of surface dimers on the Si(001)-2×1 surface in a glancing configuration.[21,23,26] However the sensitivity to the topmost layer of the surface in the normal incident experiment is not guaranteed, because the emitter can be any atom in the first few layers within the electron skin depth.

Fourth, it is very interesting to see whether the atomic

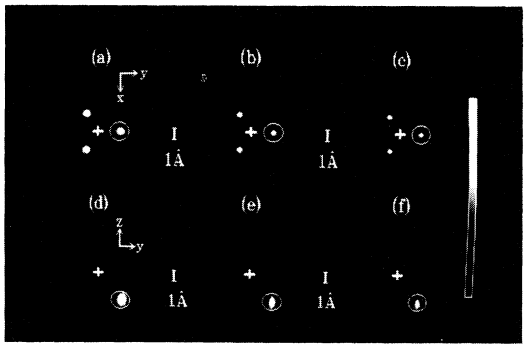

FIG. 9. Panels (a)–(c) show top-view atomic images of the Ag(111) surface at 2.35 Å below the emitter, which are reconstructed, respectively, from 11 Kikuchi patterns and with three different energy regions, i.e., 229–426, 426–686, and 686–1007 eV. Panels (d)–(f) show the side view of atomic images in (a)–(c), which are cut along the direction [01$\bar{1}$] and through the emitter.

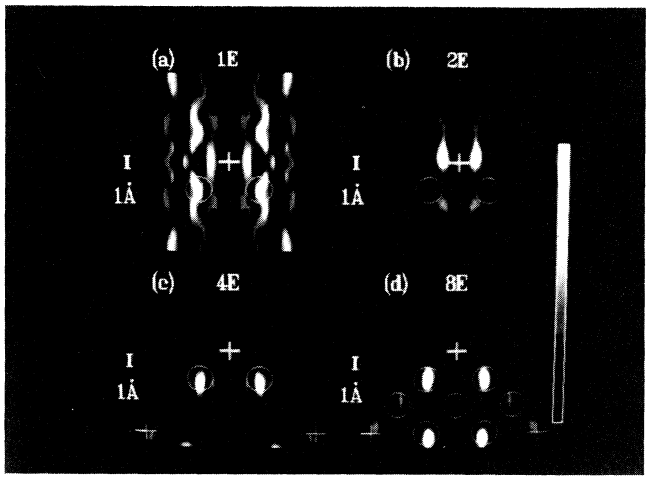

FIG. 10. Side-view atomic images of the Ag(100) surface. Panels (a)–(d) correspond to the reconstructed atomic images by inverting different numbers of Kikuchi patterns. The numbers of energies of panels (a)–(d) correspond to 1, 2, 4, and 8.

images reconstructed from the different energy regions have any difference. Shown in Figs. 9(a)–9(c) are the three top-view atomic images of the Ag(111) surface obtained by inverting 11 Kikuchi patterns with equal electron wave-number increments of $\Delta k = 0.15$ a.u.$^{-1}$ at three different energy regions, i.e., 229–426, 426–686, and 686–1007 eV. Figures 9(d)–9(f) show three side-view atomic images, which correspond, respectively, to Figs. 9(a)–9(c), and cut through the emitter and along the [01$\bar{1}$] direction. These three pairs of atomic images do not have any significant differences, however, the resolution improves as the energy region becomes higher. This is due to the fact that in the high-energy region the range of $k_{\parallel}$ (electron momentum parallel to the surface) used in the Fourier transformation is wider than in the low-energy region.

It is clear that the images in Figs. 9(d)–9(f) are all in the backward direction of the emitter, even in the high-energy region of $\sim$1000 eV where forward scattering dominates. We also found that the quality of the reconstructed images is lost when the incident energy is increased beyond 1000 eV, where the forward focusing effect dominates completely. These facts indicate that the holographic image is due to energy-dependent oscillations of outgoing electron intensity rather than the large forward focusing intensity distribution. In fact, we reconstructed 3D atomic images using the multiple-wave-number method[19] with three different energy regions, i.e., 229–426, 426–686, and 686–1007 eV, for comparison. However, we did not obtain reliable atomic images in the forward direction, as previous authors did.[20]

It is shown in Ref. 9 that the energy-dependent oscillations of the Kikuchi electron intensity at six different directions are relatively small for the energy of Kikuchi electron higher than 1000 eV. Only in the energy region between 200 and 1000 eV, can the clear intensity oscillations be acquired in all directions. This is why high-fidelity and artifact-free 3D holographic images (Fig. 9) are obtained in an energy region between 200 and 1000 eV if the integral-energy phase-summing method[9–11] is used in Fourier reconstruction.

Finally, we would like to demonstrate the importance of integral-energy phase summing[9–11] in electron-emission holography. Figures 10(a)–10(d) show side-view images of the Ag(100) crystal with different numbers of Kikuchi patterns included in the analysis. The numbers of Kikuchi patterns used in the reconstruction process are 1, 2, 4, and 8 in the energy range between 313 and 465 eV. It can be seen that there are almost no discernible atomic images in Fig. 10(a), where only a single Kikuchi pattern is used in the reconstruction. The images of the atoms become clearer when the number of Kikuchi patterns is increased. The artifacts and twins are also highly suppressed in the multiple-energy analysis. These results clearly demonstrate that one cannot have clear reconstructed atomic images with a single-energy experiment. This observation is different from the idea of direct image reconstruction of single-energy optical holography, and consistent with the strong multiple-scattering nature of the electron wave inside matter.

VI. SUMMARY

Electron-emission holography by inverting multiple-energy quasielastically scattered electron-diffraction patterns is demonstrated experimentally to fit the three basic characteristics of a direct method for surface structural determination.

It is found that most of the electrons contributed to the reconstructed images are those backward scattered from the object atoms. The fast intensity oscillation of the backward-scattered electrons as a function of electron energy is the key for observing highly resolved atomic images. Atoms in the backward direction are imaged when a limit energy range ($\sim$200 eV) of Kikuchi electrons is used. Forward-scattering images can only be observed with a large energy range ($\sim$300 eV). The sensitivity to

the local structure in the same atomic layer containing the emitter is demonstrated in an off-normal incident and detection experiment. The data treatment is simple and straightforward in IEPSM. The background subtraction in the one-dimensional energy direction is of key importance to obtain a high-fidelity 3D image. IEPSM is a general data procession, and is applicable to other kinds of electron-emission holography.

Compared with photoelectron holography, Kikuchi electron holography has one drawback, i.e., the chemical identity of the atoms cannot be specified. However, the experimental setup and time span of Kikuchi electron holography are much less complicated than those of photoelectron holography, and no synchrotron radiation light source and reliable beamline are needed. Thus one could easily perform the normal-incidence and off-normal-incidence experiments for one system in an in-house laboratory. Utilizing directional selectivity of the off-normal-incident experiments, one can possibly determine the atomic structures of complicated systems such as metal/semiconductor interfaces.

The resolution of electron-emission holography is limited to ~ 0.5 A, which cannot compare with that of conventional methods such as LEED. However, EEH is a direct method and can easily be used to determine the surface structure model. The detailed bond length and angle have to be determined by comparing the calculations of quantum-mechanical multiple scattering with the experimental results of diffraction techniques.

ACKNOWLEDGMENTS

This work was supported by the National Science Council, Republic of China, under Grant Nos. NSC-82-0208-M-001-152 and NSC-82-0208-M-007-111. We acknowledge S. Y. Tong, and W. N. Mei for helpful discussions.

[1]J. J. Barton, Phys. Rev. Lett. **61**, 1356 (1988).
[2]G. R. Harp, D. F. Saldin, and B. P. Tonner, Phys. Rev. B **42**, 9199 (1990).
[3]S. Thevuthasan, R. X. Ynzunza, E. D. Tober, C. S. Fadley, A. P. Kaduwela, and M. A. Van Hove, Phys. Rev. Lett. **70**, 595 (1993).
[4]P. Hu and D. A. King, Nature **353**, 831 (1991).
[5]D. K. Saldin, G. R. Harp, and X. Chen, Phys. Rev. B **48**, 8234 (1993).
[6]D. K. Saldin and P. L. Andres, Phys. Rev. Lett. **64**, 1270 (1990).
[7]M. A. Mendez, C. Glück, J. Guerrero, P. L. de Andres, K. Heinz, D. K. Saldin, and J. B. Pendry, Phys. Rev. B **45**, 9402 (1992).
[8]G. R. Harp, D. K. Saldin, and B. P. Tonner, Phys. Rev. Lett. **65**, 1012 (1990).
[9]C. M. Wei, I. H. Hong, P. R. Jeng, S. C. Shyu, and Y. C. Chou, Phys. Rev. B **49**, 5109 (1994).
[10]S. Y. Tong, H. Huang, and C. M. Wei, Phys. Rev. B **46**, 2452 (1992).
[11]C. M. Wei and S. Y. Tong, Surf. Sci. Lett. **274**, L577 (1992).
[12]B. P. Tonner, Zhi-Lan Han, G. R. Harp, and D. K. Saldin, Phys. Rev. B **43**, 1442 (1991).
[13]S. Y. Tong, C. M. Wei, T. C. Zhao, H. Huang, and H. Li, Phys. Rev. Lett. **66**, 60 (1991).
[14]P. Hu and D. A. King, Phys. Rev. B **46**, 13 615 (1992).
[15]S. Y. Tong, H. Li, and H. Huang, Phys. Rev. Lett. **67**, 3102 (1992).
[16]J. J. Barton, Phys. Rev. Lett. **67**, 3106 (1992).
[17]H. Li and S. Y. Tong, Surf. Sci. **282**, 380 (1993).
[18]H. Wu, G. J. Lapeyre, H. Huang, and S. Y. Tong, Phys. Rev. Lett. **71**, 251 (1993).
[19]L. J. Terminello, J. J. Barton, and D. A. Lapiano-Smith, Phys. Rev. Lett. **70**, 599 (1993).
[20]C. H. Wei, I. H. Hong, P. R. Jeng, S. C. Shyu, and Y. C. Chou, Chem. Phys. Lett. **228**, 513 (1994).
[21]I. H. Hong, P. R. Jeng, S. C. Shyu, Y.C. Chou, and C. M. Wei, Surf. Sci. Lett. **312**, L743 (1994).
[22]Z. Hussian, D. A. Shirley, C. H. Li, and S. Y. Tong, Proc. Natl. Acad. Sci. U.S.A. **78**, 5293 (1981).
[23]C. M. Wei, I. H. Hong, and Y. C. Chou, Surf. Rev. Lett. **1**, 335 (1994).
[24]H. Zhao, S. P. Tear, A. H. Jones, and D. M. Hobday, Surf. Sci. Lett. **315**, L1007 (1994).
[25]H. C. Poon, D. Snider, and S. Y. Tong, Phys. Rev. B **33**, 2198 (1986).
[26]I. H. Hong, S. C. Shyu, Y. C. Chou, and C. M. Wei (unpublished).
[27]Ph. Hofmann, K. M. Schindler, V. Fritzsche, S. Bao, A. M. Bradshaw, and D. P. Woodruff, J. Vac. Sci. Technol. A **12**, 2045 (1994).

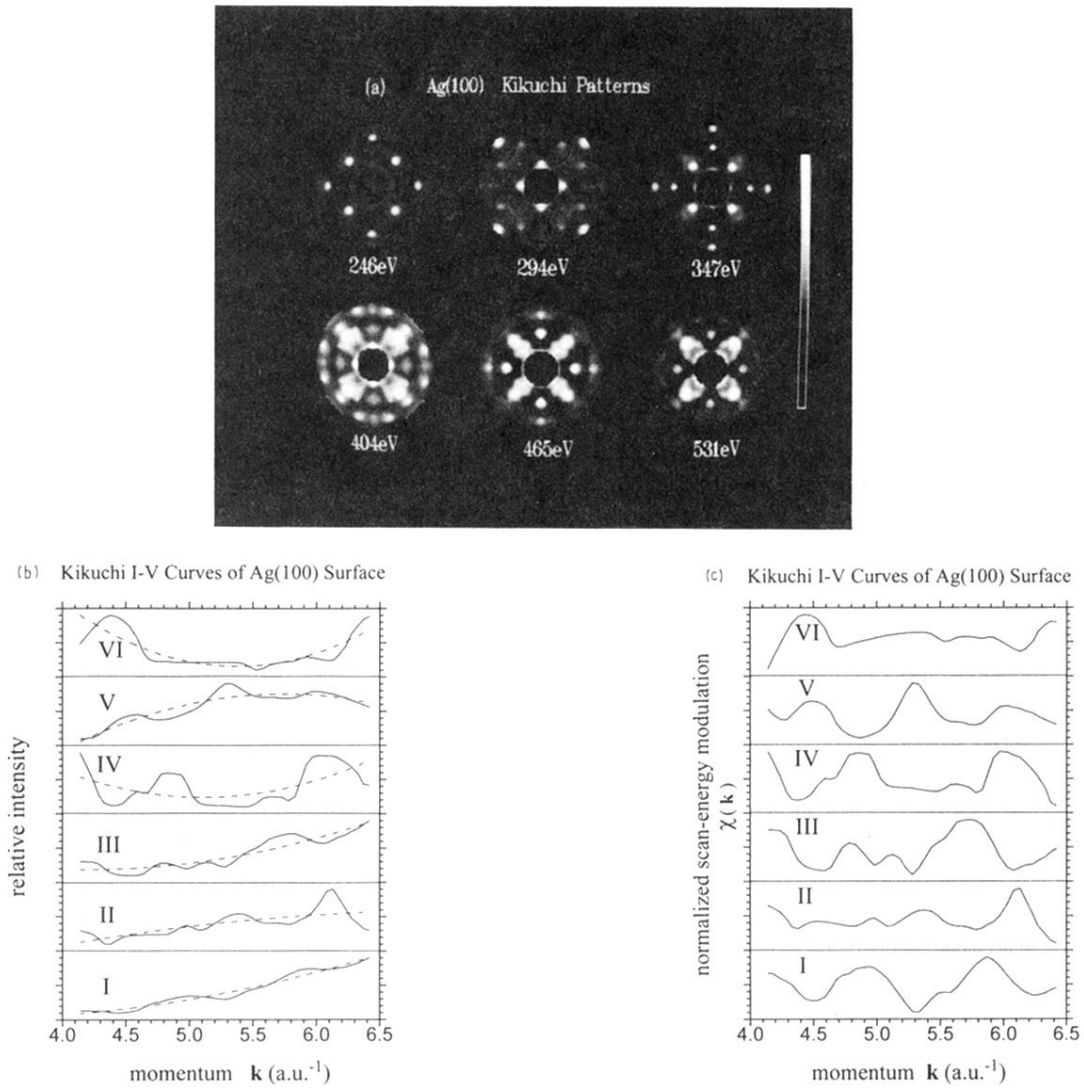

FIG. 1. (a) Six Kikuchi patterns of the Ag(100) surface at different incident energies. These patterns are displayed in an orthographic projection, with the polar angles ranging from 10° to 52°. Each pattern is fourfold symmetry averaged. The big black dot at the center of each pattern is the shadow of the electron gun. (b) The measured Kikuchi intensity spectra $I(\mathbf{k}_f)$ (solid lines) for the Ag(100) surface at six different emission directions, i.e., (I) $\varphi=0°$, $\vartheta=12.5°$; (II) $\varphi=0°$, $\vartheta=32.5°$; (III), $\varphi=15°$, $\nu=17.5°$; (IV) $\varphi=15°$, $\vartheta=37.5°$; (V) $\varphi=30°$, $\vartheta=12.5°$; and (VI) $\varphi=35°$, $\vartheta=32.5°$. The backgrounds $I_a(\mathbf{k}_f)$ (dashed lines) fitted with the second-order polynomial. (c) The normalized intensity modulations $\chi(\mathbf{k}_f)$ of Kikuchi electrons for the Ag(100) surface at the same six emission directions reported in (b).

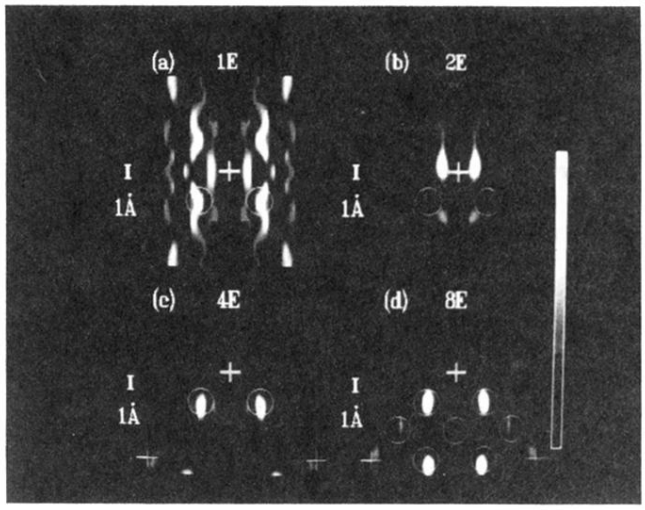

FIG. 10. Side-view atomic images of the Ag(100) surface. Panels (a)–(d) correspond to the reconstructed atomic images by inverting different numbers of Kikuchi patterns. The numbers of energies of panels (a)–(d) correspond to 1, 2, 4, and 8.

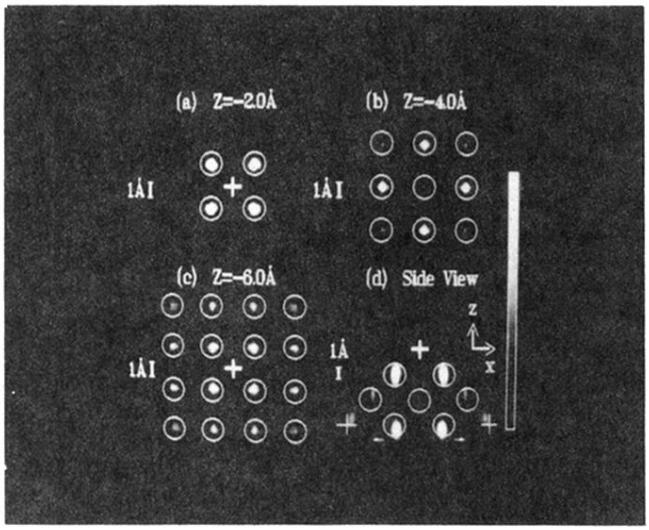

FIG. 2. The top-view atomic images of the Ag(100) surface below the emitter at (a) 2.0 Å, (b) 4.0 Å, and (c) 6.0 Å. (d) The side-view reconstructed image of the Ag(100) surface cut through the (001) plane of the images shown in (a)–(c). Complete 3D holographic images are shown in Fig. 4(a).

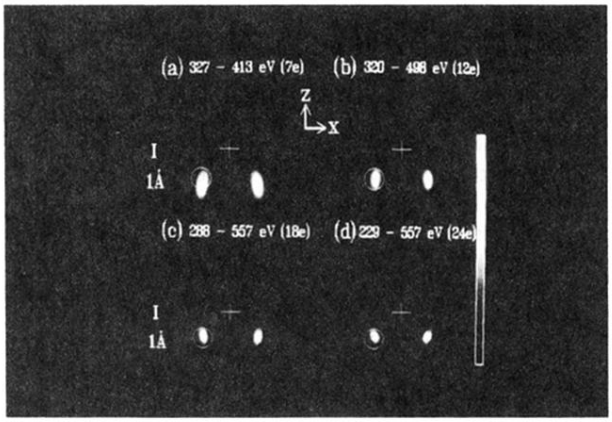

FIG. 3. Atomic images of the Ag(100) surface for various numbers of Kikuchi patterns in the image reconstruction.

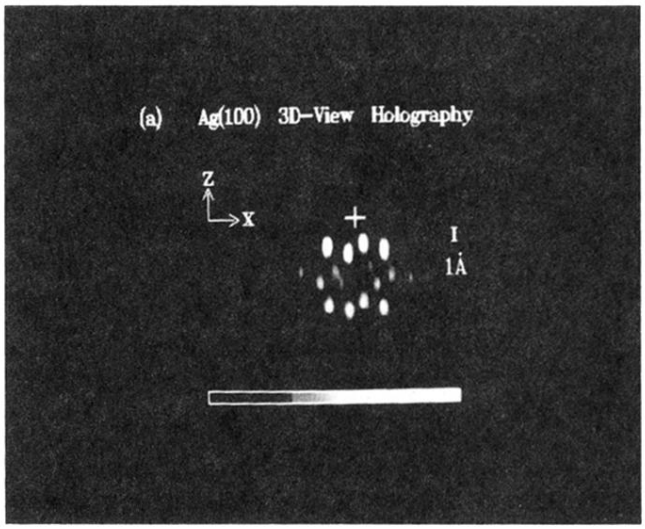

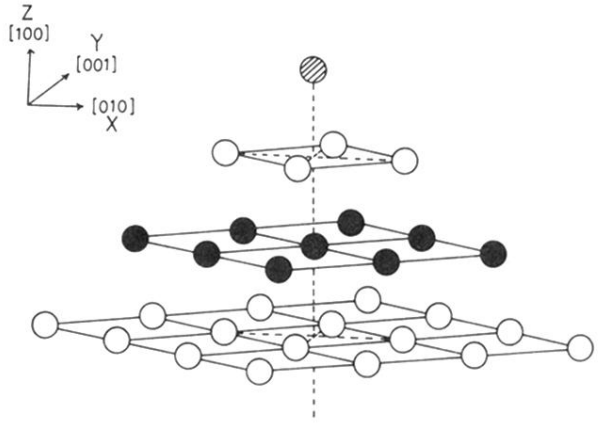

(b)

FIG. 4. (a) The 3D view of atomic images of the Ag(100) surface reconstructed from eight Kikuchi patterns (313–465 eV). Atoms down to three layers below the emitter (marked by thick cross) are observed. (b) The 3D view of the atomic structural diagram of the Ag(100) surface.

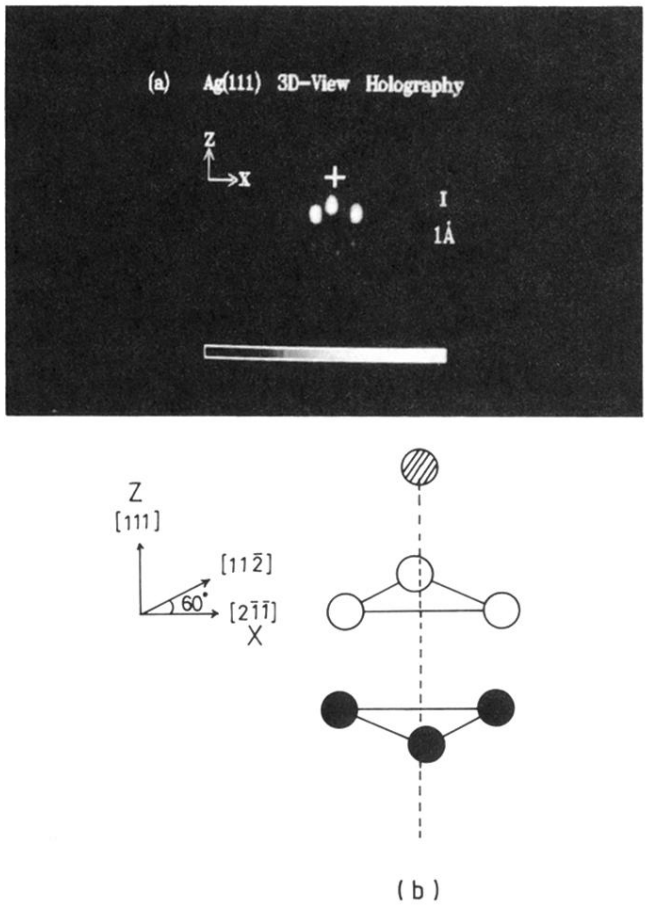

FIG. 5. (a) The 3D view of atomic images of the Ag(111) surface reconstructed from 11 Kikuchi patterns (300–548 eV). (b) The 3D view of the atomic structural diagram of the Ag(111) surface.

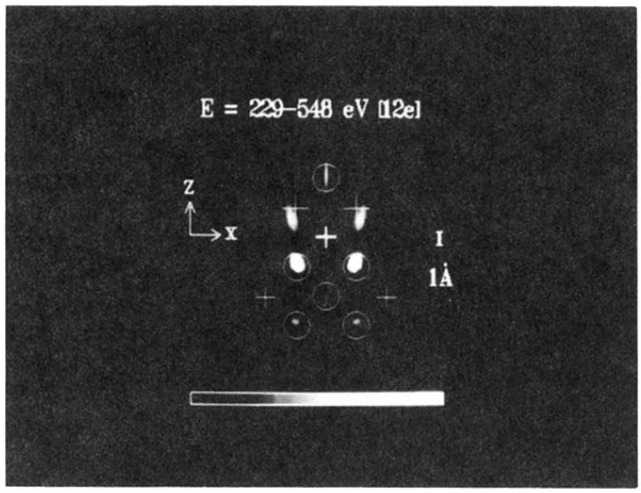

FIG. 7. Side-view atomic images along the (001) plane of the Ag(100) surface reconstructed with a wider energy range of 229–548 eV. Both the backward- and forward-scattering atomic images are observed.

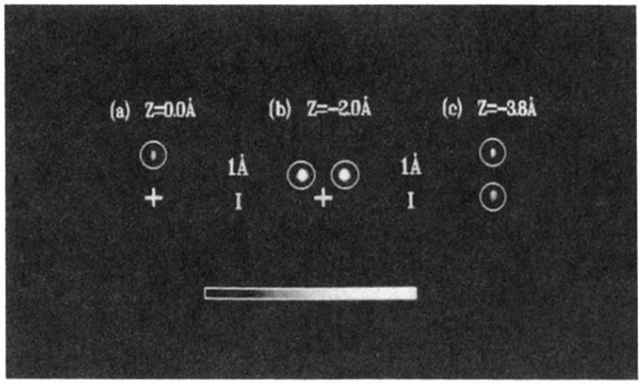

FIG. 8. The top-view atomic images of the Ag(100) surface below the emitter for an off-normal incident geometry (see the text). Panels (a)–(c) correspond to three different layers: (a) at 0.0 Å, (b) at 2.0 Å, and (c) at 3.8 Å. These images are reconstructed from 11 Kikuchi patterns (234–457 eV).

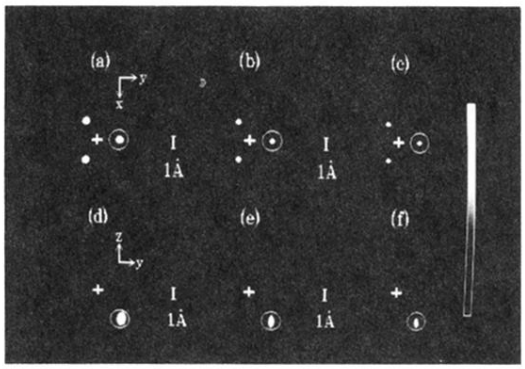

FIG. 9. Panels (a)–(c) show top-view atomic images of the Ag(111) surface at 2.35 Å below the emitter, which are reconstructed, respectively, from 11 Kikuchi patterns and with three different energy regions, i.e., 229–426, 426–686, and 686–1007 eV. Panels (d)–(f) show the side view of atomic images in (a)–(c), which are cut along the direction $[01\bar{1}]$ and through the emitter.